RECENT RESULTS FROM PHOBOS AT RHIC

EDMUNDO GARCIA[6*]
FOR THE PHOBOS COLLABORATION
B.B.BACK[1], M.D.BAKER[2], M.BALLINTIJN[4], D.S.BARTON[2], R.R.BETTS[6], A.A.BICKLEY[7], R.BINDEL[7], W.BUSZA[4], A.CARROLL[2], Z.CHAI[2], M.P.DECOWSKI[4], E.GARCIA[6], T.GBUREK[3], N.GEORGE[2], K.GULBRANDSEN[4], C.HALLIWELL[6], J.HAMBLEN[8], M.HAUER[2], C.HENDERSON[4], D.J.HOFMAN[6], R.S.HOLLIS[6], R.HOŁYŃSKI[3], B.HOLZMAN[2], A.IORDANOVA[6], E.JOHNSON[8], J.L.KANE[4], N.KHAN[8], P.KULINICH[4], C.M.KUO[5], W.T.LIN[5], S.MANLY[8], A.C.MIGNEREY[7], R.NOUICER[2,6], A.OLSZEWSKI[3], R.PAK[2], C.REED[4], C.ROLAND[4], G.ROLAND[4], J.SAGERER[6], H.SEALS[2], I.SEDYKH[2], C.E.SMITH[6], M.A.STANKIEWICZ[2], P.STEINBERG[2], G.S.F.STEPHANS[4], A.SUKHANOV[2], M.B.TONJES[7], A.TRZUPEK[3], C.VALE[4], G.J.VAN NIEUWENHUIZEN[4], S.S.VAURYNOVICH[4], R.VERDIER[4], G.I.VERES[4], E.WENGER[4], F.L.H.WOLFS[8], B.WOSIEK[3], K.WOŹNIAK[3], B.WYSŁOUCH[4]

[1] *Argonne National Laboratory, Argonne, IL 60439-4843, USA*
[2] *Brookhaven National Laboratory, Upton, NY 11973-5000, USA*
[3] *Institute of Nuclear Physics PAN, Kraków, Poland*
[4] *Massachusetts Institute of Technology, Cambridge, MA 02139-4307, USA*
[5] *National Central University, Chung-Li, Taiwan*
[6] *University of Illinois at Chicago, Chicago, IL 60607-7059, USA*
[7] *University of Maryland, College Park, MD 20742, USA*
[8] *University of Rochester, Rochester, NY 14627, USA*

The PHOBOS detector is one of four heavy-ion experiments at the Relativistic Heavy Ion Collider (RHIC) at Brookhaven National Laboratory. In this paper we will review some of the results of PHOBOS from the data collected in p+p, d+Au and Au+Au collisions at nucleon-nucleon center-of-mass energies up to 200 GeV. In the most central Au+Au collisions at the highest energy, evidence is found for the formation of a very high energy density and highly interactive system, which can not be described in terms of hadrons, and which has a relatively low baryon density.

*Corresponding author, e-mail: ejgarcia@uic.edu

1. Introduction

The bulk of the hadronic matter is made of quarks and gluons (partons), bound into neutrons and protons. These hadrons then form nuclear structures held together by the strong interactions mediated by the gluons. The fundamental interactions between partons are well described by the theory of Quantum Chromodynamics (QCD). However, due to the non-commutative nature of the parton interactions, the phase structure of strongly interacting matter is only partially understood in terms of QCD. The knowledge we have of the properties of strongly interacting matter comes from experimental data.

At distances close to the hadronic size, the QCD coupling constant decreases with decreasing distance between the partons. As a consequence it is expected that at high temperatures a parton conglomerate should have properties of an ideal relativistic gas [1], traditionally designated as the Quark-Gluon Plasma (QGP). The transition between the QGP and the strongly interacting matter that exist at normal temperature and density (protons and neutrons) happens, according to QCD, with the spontaneous breaking of "chiral symmetry" and "deconfinement" [2].

Lattice gauge calculations suggest that at low baryon densities there is a phase differentiation in a highly interactive matter below and above a critical temperature $T_c \sim 170$ MeV, or energy density $\epsilon \sim 1$ GeV/fm^3 [3]. The closest approach to the creation of matter under these conditions is achieved in relativistic heavy-ion collisions. The most recent facility for the study of these collisions is the Relativistic Heavy Ion Collider (RHIC). Four experiments at RHIC have studied the collisions of p+p, Au+Au and d+Au systems at nucleon-nucleon center-of-mass energies, $\sqrt{s_{NN}}$, from 19.6 GeV to 200 GeV. Data from these experiments are being studied to get a better understanding of the physics of heavy-ion collisions and in particular to search for the evidence of the phase transition of the highly interactive parton matter or QCD matter. This paper summarizes some of the results obtained by the PHOBOS collaboration.

The PHOBOS apparatus is composed of three major subsystems; a charged particle multiplicity detector covering almost the entire solid angle; a two arm magnetic spectrometer with particle identification capability, and a suite of detectors used for triggering and centrality determination. A full description of the PHOBOS detector and its properties can be found in Ref. [4]. Also, a description of some of the techniques used for the PHOBOS event selection (triggering) and event characterization (vertex position and

centrality of the collision) can be found in Ref. [5].

2. The formation of a very high energy density state at RHIC

Figure 1 shows the evolution of the midrapidity charged particle density $dN_{ch}/d\eta\rfloor_{|\eta|\leq 1}$, per participating nucleon pair, $N_{part}/2$, as a function of $\sqrt{s_{_{NN}}}$ [6]. The data are consistent with a logarithmic extrapolation from lower energies as shown by the solid line drawn in the plot. The mid rapidity particle density at $\sqrt{s_{_{NN}}}$= 200 GeV is almost a factor of two higher than the value observed at the maximum SPS energy. The details of the evolution of the charged particle pseudorapidity density are shown in Fig. 2, where $dN_{ch}/d\eta$ is presented for Au+Au collisions at $\sqrt{s_{_{NN}}}$=19.6, 130, and 200 GeV for various centralities [7]. The particle densities peak near midrapidity and increase with both $\sqrt{s_{_{NN}}}$ and centrality.

An approximation of the total energy density in the system created at midrapidity in Au+Au collisions at $\sqrt{s_{_{NN}}}$=200 GeV can be calculated from the charged particle pseudorapidity density, the average energy per particle and the volume from where the system was originated. Figure 3 shows the transverse momentum distributions of identified particles emitted at mid rapidity in central Au+Au collisions at $\sqrt{s_{_{NN}}}$=200 GeV. The yield at low transverse momentum (p_T) was measured by PHOBOS [8] and the high p_T data was measured by PHENIX [9]. Fits to the yield make it possible to estimate the average transverse mass for all charged particles, $\langle m_T \rangle \simeq 600$ MeV/c, which is equal to the transverse energy at midrapidity. Under the assumption of a spherically symmetric distribution in momentum space, which would have equal average transverse and longitudinal momenta.

As for the volume where the system originated, elliptic flow results discussed below suggest that an upper limit of the time for the system to reach approximate equilibrium is of the order of 1–2 fm/c. Using the upper range of this estimate and assuming that the system expands during this time in both longitudinal and transverse directions one obtains a conservative estimate for the energy density produced at RHIC when the system reaches approximate equilibrium of $\epsilon \geq 3$ GeV/fm^3. This estimate is about 6 times the energy density inside the nucleons. Thus, a very high energy system is created whose description in terms of hadronic degrees of freedom is inappropriate.

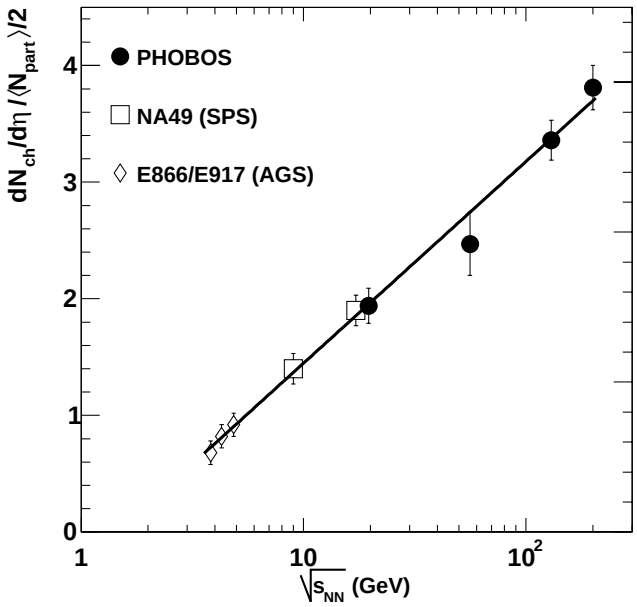

Figure 1. Evolution of the midrapidity charged particle density $dN_{ch}/d\eta\rfloor_{|\eta|\leq 1}$, per participating nucleon pair, $N_{part}/2$, as a function of collision energy. Solid line is a logarithmic extrapolation of the data from lower energies drawn to guide the eye.

3. Baryon chemical potential at RHIC energies: Approach to a baryon free environment

One of the most interesting results from heavy-ion collisions at lower energies was the observation that the production ratios for different particles with cross-section varying over several orders of magnitude can be described in terms of a statistical picture of particle production assuming chemical equilibrium [10]. One of the key components in the particle production mechanism is the baryon chemical potential μ_B which can be extracted from the kaon to antikaon and proton to antiproton ratios. The measurement of the ratios of charged antiparticles to particles produced at RHIC is shown in Fig. 4. This figure compares the antiparticle to particle ratios for both kaons and protons to the corresponding data at lower energies [11].

The system formed at RHIC is closer to having equal number of particles and antiparticles than that found at lower energies. The measured ratio for antiproton to proton production as function of the energy indicates that

the system approaches smaller values of μ_B at higher energies. Assuming a hadronization temperature of 160–170 MeV, a value of $\mu_B = 27$ MeV was found for central Au+Au collisions at $\sqrt{s_{NN}}$=200 GeV, showing that the system created at RHIC is close to a baryon-free medium.

4. Interaction strength in high energy density medium

The medium produced in heavy-ion collisions at RHIC energies was initially thought to consist of a weekly interacting plasma of quarks and gluons [12]. From experimental evidence it has been found however, that the nature of the system formed is not weakly interacting. As shown in Fig. 3, the production of particles with low p_T is consistent with the extrapolations from a fit to the distributions in the range from around 200 MeV to few GeV. If at RHIC, a medium of weakly interacting particles was formed, one would expect an enhancement of the production of particles with wavelengths roughly equal to the size of the collision volume (coherent pion production) [13]. The absence of an excess of particles at low transverse momentum is a manifestation of the strongly interacting nature of the medium produced at RHIC, which also gives rise to a large radial and elliptic flow signal.

Figure 5 shows the magnitude of elliptic flow (v_2) measured by PHOBOS around midrapidity ($|\eta| \leq 1$) in Au+Au collisions at $\sqrt{s_{NN}}$=130 GeV and 200 GeV as a function of the number of participants (N_{part}) [14,15]. The elliptic flow signal is strong over a wide range in centrality and close to the value predicted by a relativistic hydrodynamics calculation [18]. The observation of an azimuthal asymmetry in the out-going particles is evidence of early interactions. Furthermore, from the strength of the observed elliptic flow and the known dimensions of the overlap region it can be estimated that the initially formed medium equilibrates in a time less than about 2 fm/c [16], the value used earlier in the calculation of the energy density.

Figure 6 shows the yield of charged particles per participant pair divided by a fit to the invariant cross section for proton-antiproton collisions (200 GeV UA1 [17]) plotted as a function of p_T, for the most peripheral and most central interactions. The dashed and solid lines show the expectation of the scaling of yields with the number of collisions ($\langle N_{coll} \rangle$) and the number of participants $\langle N_{part} \rangle$, respectively. The brackets show the systematic uncertainty. We can see that the general shape of the curves is only weakly dependent on the centrality and for p_T values up to 2 GeV/c there is an increase of the yield in Au+Au collisions compared to $\mathrm{p\bar{p}}$. Above 2 GeV/c, the relative yield decreases for all centrality bins.

Two possible explanations have been suggested for this yield suppression as function transverse momentum relative to N_{coll} scaling for central collisions. The first ("initial state") model suggests that the effect is due to a modification of the wave functions of the nucleons in the colliding ions. This produces an effective increase of the interaction length in such a way that the nucleons in a nucleus will interact coherently with all the nucleons in the other nucleus in the longitudinal dimension [19]. This model predicts not only the yield quenching at high p_T, but also the scaling of the yield with the number of participants. The second ("final state") model suggests that the suppression comes from an increase of the energy loss of the partons traveling through the hot dense medium formed in the Au+Au collisions [20]. One way to discriminate between these models is to reduce the size of the hot and dense medium, by colliding d+Au instead of Au+Au. RHIC's 2003 run was dedicated mainly to d+Au collisions at $\sqrt{s_{NN}}$ = 200 GeV. Details of the analysis and a broader discussion of p_T spectra are given in Ref. [21].

In Fig. 7 we present the nuclear modification factor R_{dAu} as function of p_T for four centrality bins defined as the ratio of the d+Au invariant cross section divided by the $p\bar{p}$ UA1 yield, scaled by the proton-antiproton invariant cross section (41 mb) and $\langle N_{coll}\rangle$. For the centrality bins there is a rapid rise of R_{dAu} reaching a maximum at around p_T= 2 GeV/c. For comparison, the R-factor is also plotted for the most central bin for Au+Au collisions at $\sqrt{s_{NN}}$ = 200 GeV. In striking contrast to the behavior of R_{dAu}, R_{AuAu} also increases initially as function of p_T but above 2 GeV/c it decreases sharply.

The suppression of the inclusive yield observed in central Au+Au collisions is consistent with final-state interactions with in a dense medium crated in such collisions. Thus we find that the matter created at RHIC interacts strongly with high-p_T partons as expected for a partonic medium.

5. Final remarks

In central A+Au collisions at the highest RHIC energies, a very high energy density medium is formed. Conservative estimates of its density are around 3 GeV/fm^3. This is greater than hadronic densities and it is inappropriate to describe this medium in terms of hadronic degrees of freedom. The medium has been found to have a low baryon chemical potential. The transition to this state does not create abrupt changes in any observable including charged particle multiplicity, elliptic flow, interferometric radii,

and other derived quantities which have been studied so far. This lack of strong signals will make it difficult to delineate the boundaries between high density highly interactive matter and hadronic states.

6. Acknowledgments

This work was partially supported by U.S. DOE grants DE-AC02-98CH10886, DE-FG02-93ER40802, DE-FC02-94ER40818, DE-FG02-94ER40865, DE-FG02-99ER41099, and W-31-109-ENG-38, by U.S. NSF grants 9603486, 0072204, and 0245011, by Polish KBN grant 1-P03B-062-27(2004-2007), and by NSC of Taiwan Contract NSC 89-2112-M-008-024.

References

1. D. J. Gross, R. D. Pisarski, and L. G. Yaffe, *Rev. Mod. Phys.* **53**, 43 (1981).
2. R. D. Pisarski and F. Wilczek, *Phys. Rev.* **D29**, 338 (1984).
3. F. Karsch, *Nucl. Phys.* **A698**, 199 (2002).
4. B. B. Back *et. al.*, (PHOBOS), *Nucl. Inst. Meth.* **A499**, 603 (2003).
5. B. B. Back *et. al.*, (PHOBOS), *Phys. Rev.* **C70**, 021902(R) (2004).
6. B. B. Back *et. al.*, (PHOBOS), submitted to *Nucl. Phys A*; arXiv:nucl-ex/0410022 (2004).
7. B. B. Back *et. al.*, (PHOBOS), *Phys. Rev. Lett.* **91**, 052303 (2003).
8. B. B. Back *et. al.*, (PHOBOS), submitted to *Phys. Rev. Lett.*; arXiv:nucl-ex/0401006 (2004).
9. S. S. Adler *et. al.*, (PHENIX), *Phys. Rev.* **C69**, 034909 (2004).
10. P. Braun-Munzinger *et. al.*, *Phys. Lett. B* **465**, 15 (1999).
11. B. B. Back *et. al.*, (PHOBOS), *Phys. Rev. Lett.* **87** 102301 (2001).
12. E. V. Shuryak, arXiv:hep-ph/0405066.
13. W. Busza, Proceedings of NATO Advanced Study Institute on Particle Production in Highly Excited Matter, 149 (1993).
14. B. B. Back *et. al.*, (PHOBOS), *Phys. Rev. Lett.* **89** 222031 (2002).
15. B. B. Back *et. al.*, (PHOBOS), submitted to *Phys. Rev. C (RC)*; arXiv:nucl-ex/0407012 (2004).
16. P. F. Kolb and U. Heinz, Hydrodynamical description of ultrarelativistic heavy ion collisions. *World Scientific* (2004); arXiv:nucl-th/0305084 (2003).
17. G. Arnison et al., (UA1), Phys. Lett. B 118 (1982) 167.
18. U. W. Heinz, and H. Heiselberg, *Phys. Lett.* **500**, 232 (2001).
19. D. Kharzeev, E. Levin and L. McLerran, arXiv:hep-ex/0210332 (2002).
20. M. Gyulassy, I. Vitev, X. Wang and B. Zhang arXiv:hep-ex/0302077 (2003).
21. B. B. Back *et. al.*, (PHOBOS), *Phys. Rev. Lett.* **91** 072302 (2003).

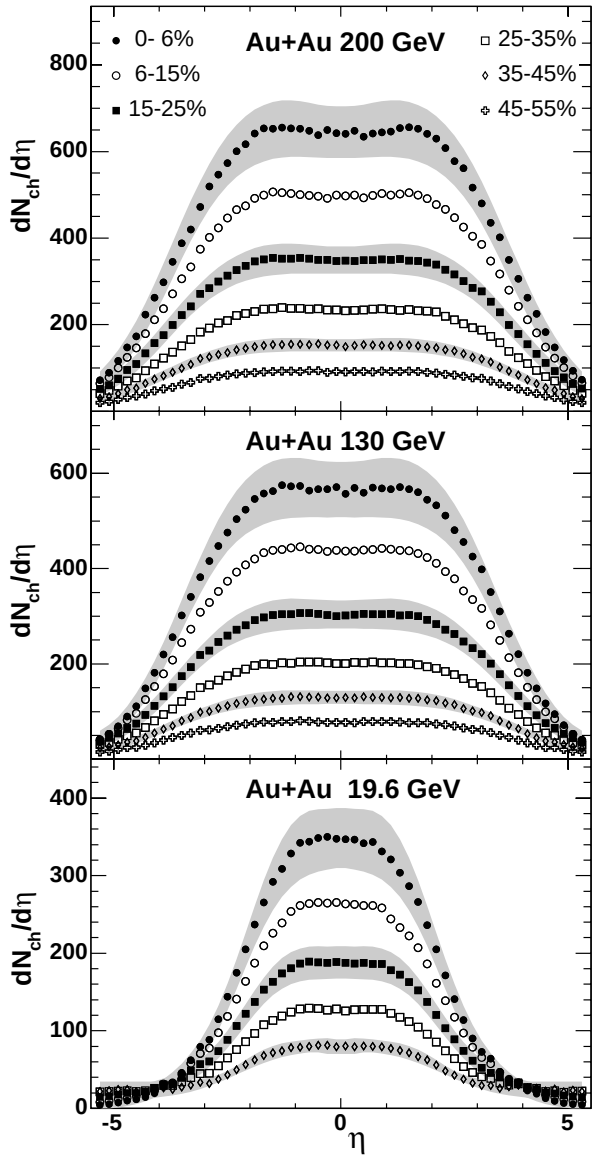

Figure 2. Pseudorapidity density of charged particles emitted in Au+Au collisions at three different values of the nucleon-nucleon center-of-mass energy. Data are shown for a range of centralities, labeled by the fraction of the total inelastic cross section in each bin, with smaller numbers being more central. Grey bands shown for selected centrality bins indicate the typical systematic uncertainties (90% C.L.). Statistical errors are smaller than the symbols.

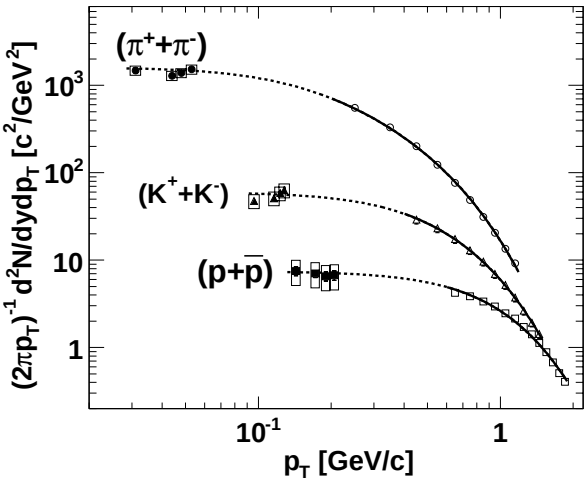

Figure 3. Transverse momentum distributions of identified charged particles emitted near midrapidity in central Au+Au collisions at $\sqrt{s_{NN}}$=200 GeV. Invariant yield data shown are from PHENIX at higher momenta and PHOBOS at lower momenta. Boxes around the PHOBOS data indicate systematic uncertainties. Fits to PHENIX measurements are shown by solid curves ($\propto 1/[e^{(m_T/T)} + \epsilon]$, where $\epsilon = -1$ and $+1$ for mesons and baryons, respectively, m_T is the transverse mass, and T is the fit parameter). Note that the extrapolations (dashed curves) of the fit to the data at higher momenta are consistent with the low momentum yields.

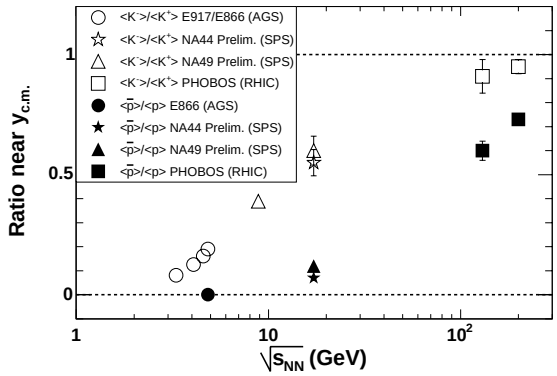

Figure 4. Ratios of identified antiparticles over particles measured near midrapidity in central collisions of Au+Au and PHOBOS at RHIC and Pb+Pb as a function of nucleon-nucleon center-of-mass energy. Error bars are statistical only.

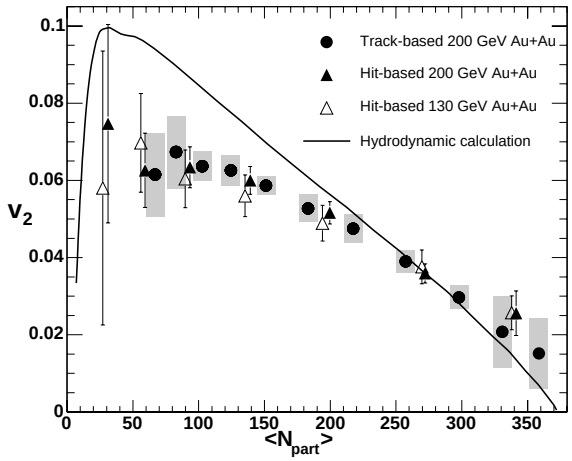

Figure 5. Elliptic flow of charged particles near midrapidity ($|\eta| < 1$) as a function of centrality in Au+Au collisions at $\sqrt{s_{NN}}$=200 GeV (closed circles and triangles, are measurement using two different analysis methods) and at $\sqrt{s_{NN}}$=130 GeV (open triangles). Grey boxes show the systematic errors (90% C.L.) for the 200 GeV data. The curve shows the prediction from a relativistic hydrodynamics calculation.

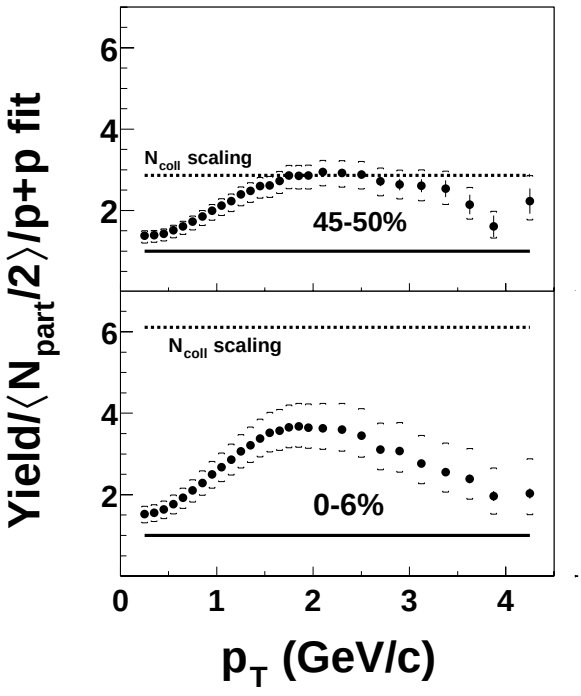

Figure 6. Ratio of the yield of charged hadrons in Au+Au as a function of p_T for the most peripheral and the most central bin to a fit of proton antiproton data scaled by $\langle N_{part}/2\rangle$. The dashed(solid) line shows the expectation of $N_{coll}(N_{part})$ scaling relative to $p\bar{p}$ collisions. The brackets show the systematic uncertainty.

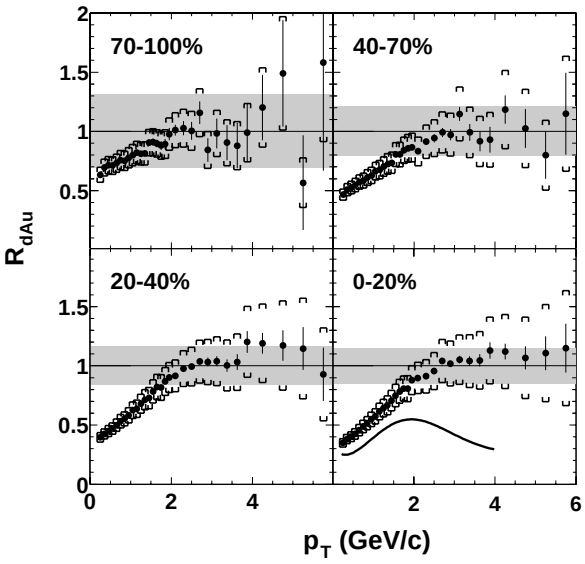

Figure 7. Nuclear modification factor R_{dAu} as a function of p_T for four centrality bins. For the most central bin, the spectral shape for central Au+Au data relative to $p + \bar{p}$ is shown for comparison. The shaded area shows the uncertainty in R_{dAu} due to the systematic uncertainty in $\langle N_{coll} \rangle$ and the UA1 scale error (90% C.L.). The brackets show the systematic uncertainty of the d+Au spectra measurement (90% C.L.).